Supporting Information

New Structurally Diverse Photoactive Cadmium Coordination Polymers†

Ning Wang,[a#] Bing-Fan Long,[a#] Xian-Hong Yin,[a] Zhong-jing Huang,[a] Yan Mi,[a] Fei-Long Hu*[a] David James Young*[b]

[a] *Key Laboratory of Chemistry and Engineering of Forest Products, State Ethnic Affairs Commission, Guangxi Key Laboratory of Chemistry and Engineering of Forest Products, Guangxi Collaborative Innovation Center for Chemistry and Engineering of Forest Products, Guangxi University for Nationalities, Nanning 530006, China*

[b] *College of Engineering, IT and Environment, Charles Darwin University, Darwin, NT 0909, Australia*

Table of contents

Experimental Section

Materials and Instruments

Analytical grade chemicals were obtained commercially and used without further purification. Elemental analyses (C, H and N) were performed using a PE 2400 II elemental analyzer. **FT-IR** spectra were recorded with a Nicolet Magna-IR 550 spectrometer on dry KBr disks in the 4000-400 cm^{-1} range. Thermogravimetric analyses (**TGA**) were performed using a Mettler TGA thermal analyzer under a N_2 atmosphere with a heating rate of 10 ^oC min^{-1} in the temperature region 20-1000 ^oC. Powder X-ray diffraction (**PXRD**) patterns were collected on a Bruker D8 advance diffractometer using graphite monochromatized Cu Kα radiation. **NMR** spectra were recorded at ambient temperature on a Bruker AVANCE 400M spectrometer. ^1H NMR chemical shifts were referenced to the solvent signal in $CDCl_3$ or d_6-DMSO. ^{13}C NMR spectra were recorded at a resonance frequency of 101.6 MHz on a Bruker AVANCE 400M spectrometer.

Single-crystal Structure Determination

Single-crystal X-ray diffraction data for **CP_1-CP_4** were recorded on a Bruker Smart CCD diffractometer with a graphite monochromated Mo Kα radiation (λ = 0.71073 Å) at 293 K. Structures were solved by Direct Methods and refined by full-matrix least-squares techniques[1-3] using the *SHELXL-2017* program[4, 5]. Non-hydrogen atoms were refined with anisotropic displacement parameters[6]. The H atoms bonded to C and N atoms were positioned with idealized geometry and refined with fixed isotropic displacement parameters.

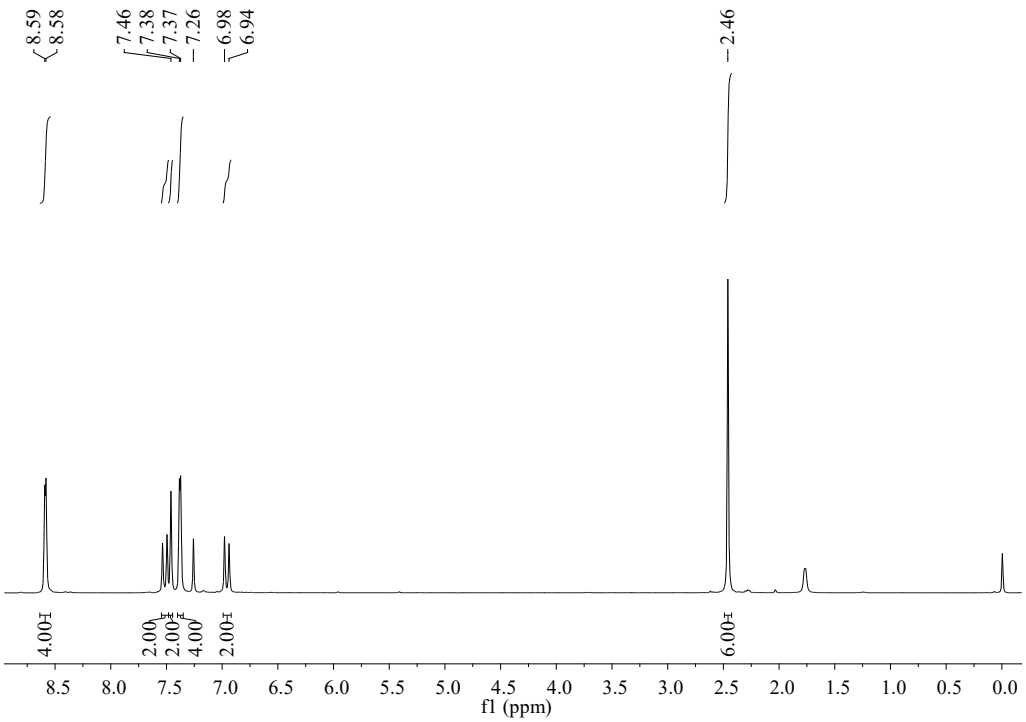

(a)

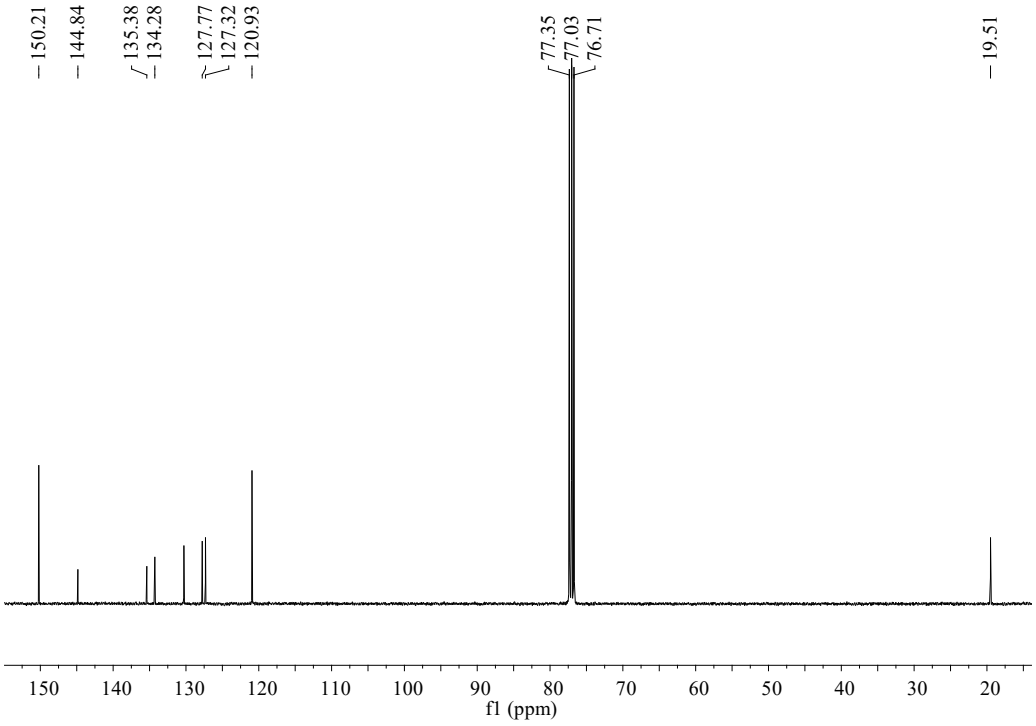

(b)

Fig. S1. ^{1}H NMR (a) and ^{13}C NMR (b) spectra of CH_3-bpeb ($CDCl_3$)

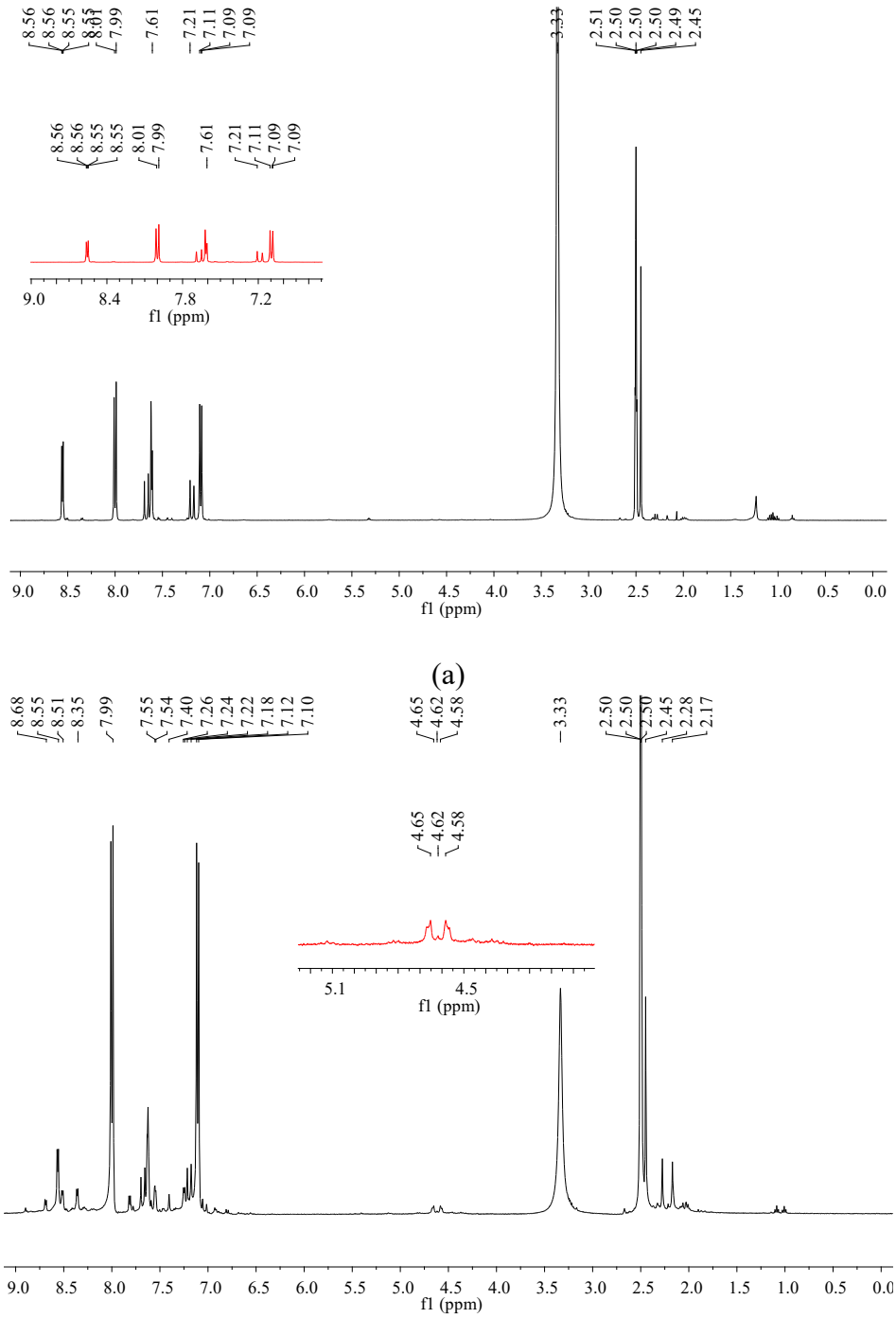

Fig. S2. The ^{1}H NMR spectra of CP_1 before UV irradiation (a) and after irradiation under UV light (b) (λ = 365 nm) (d_6-DMSO).

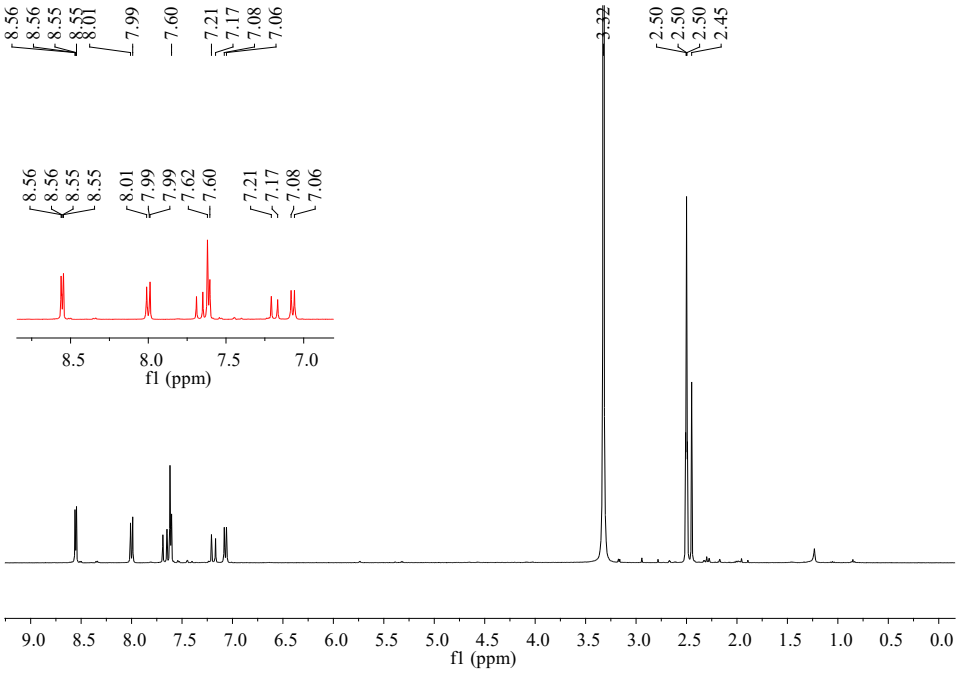

(a)

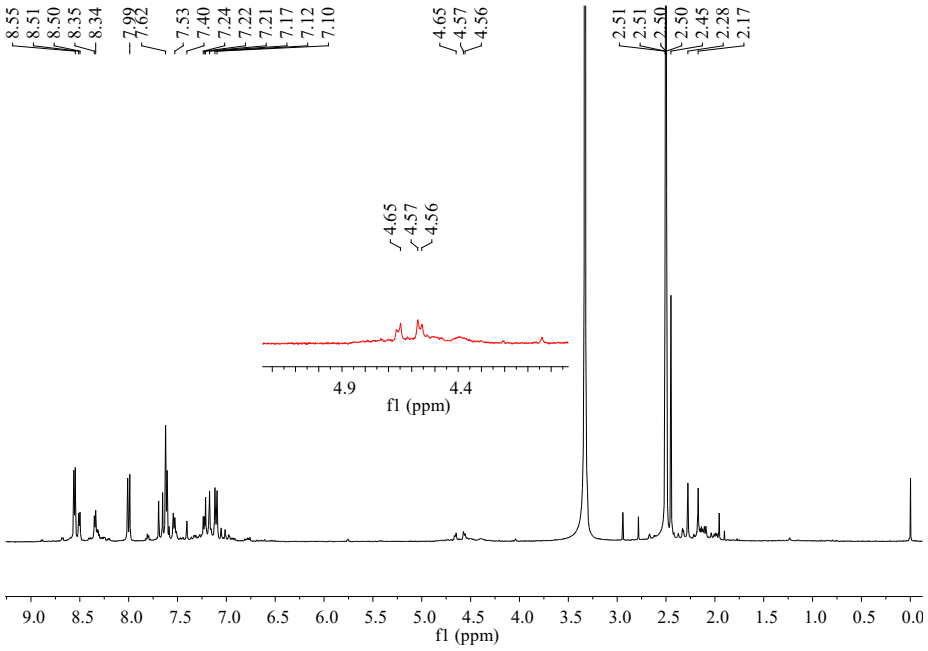

(b)

Fig. S3. The ^{1}H NMR spectra of CP_2 before UV irradiation (a) and after irradiation under UV light (b) (λ = 365 nm) (d_6-DMSO).

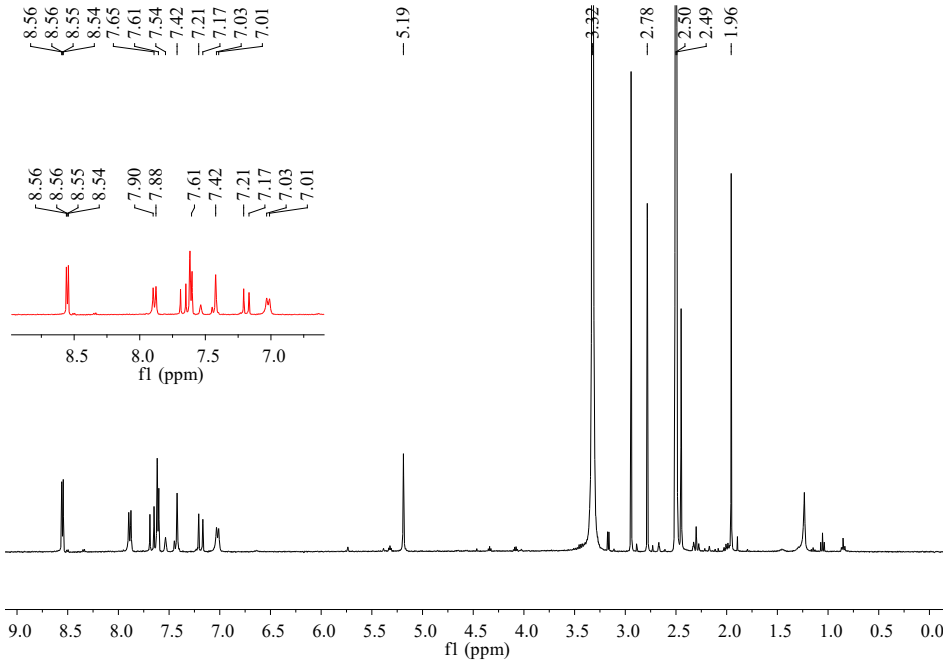

(a)

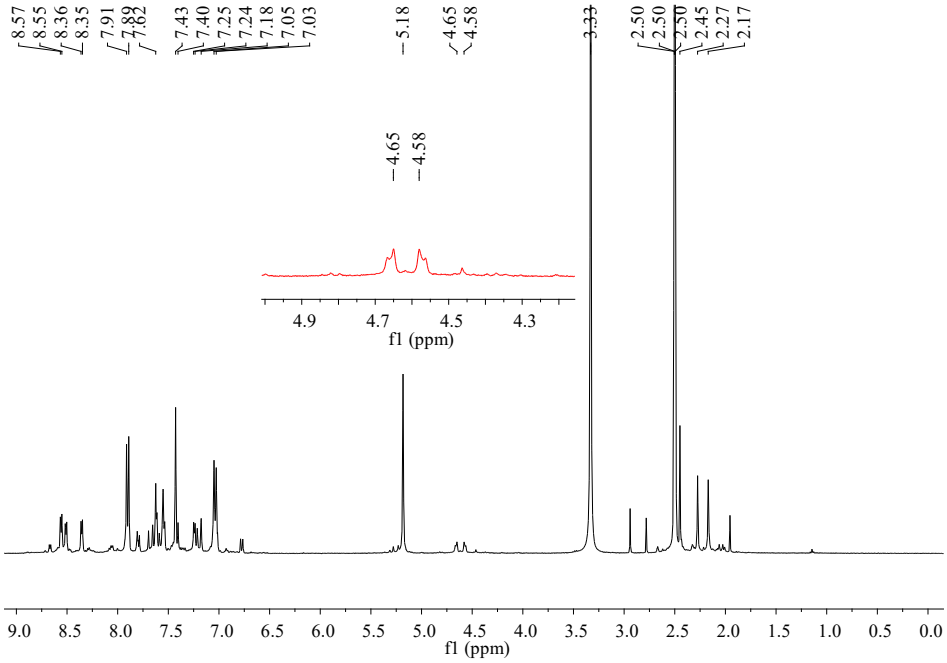

(b)

Fig. S4. The ^{1}H NMR spectra of CP_3 before UV irradiation (a) and after irradiation under UV light (b) (λ = 365 nm) (d_6-DMSO).

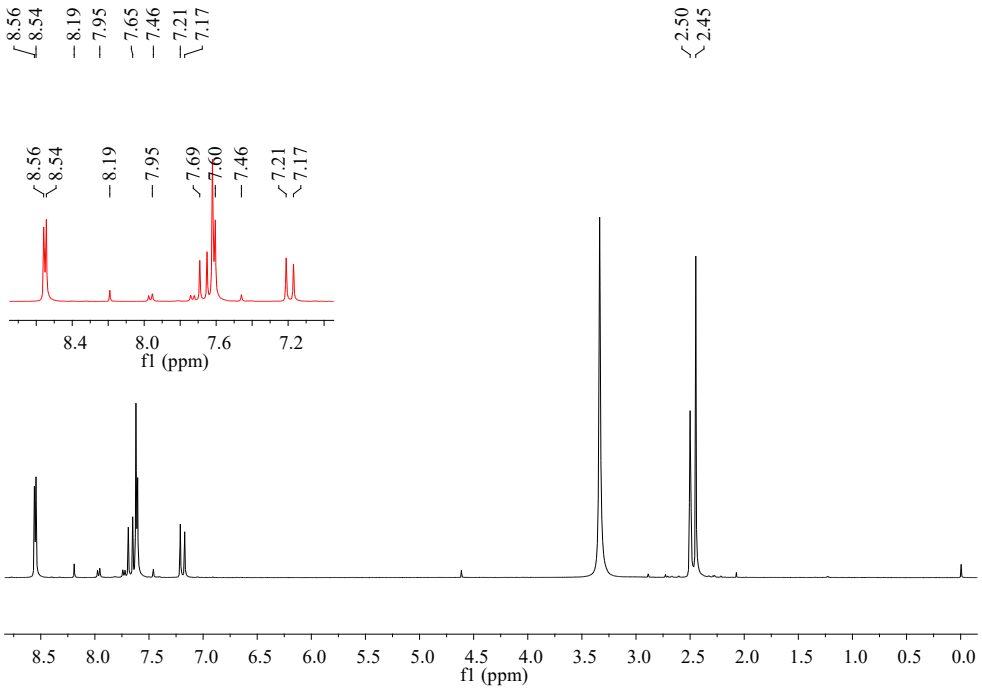

(a)

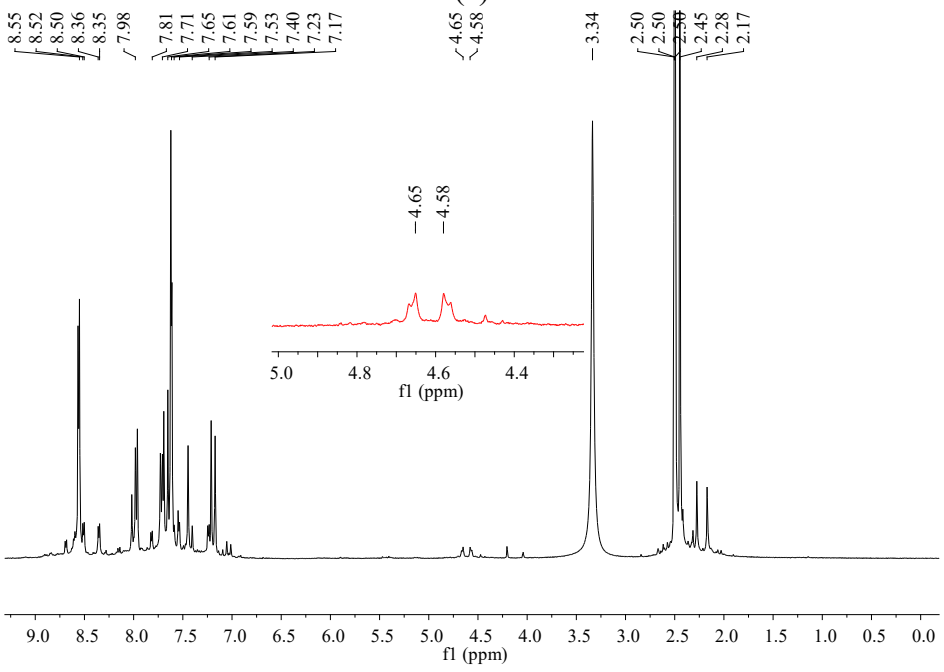

(b)

Fig. S5. The ^{1}H NMR spectra of CP_4 before UV irradiation (a) and after irradiation under UV light (b) (λ = 365 nm) (d_6-DMSO).

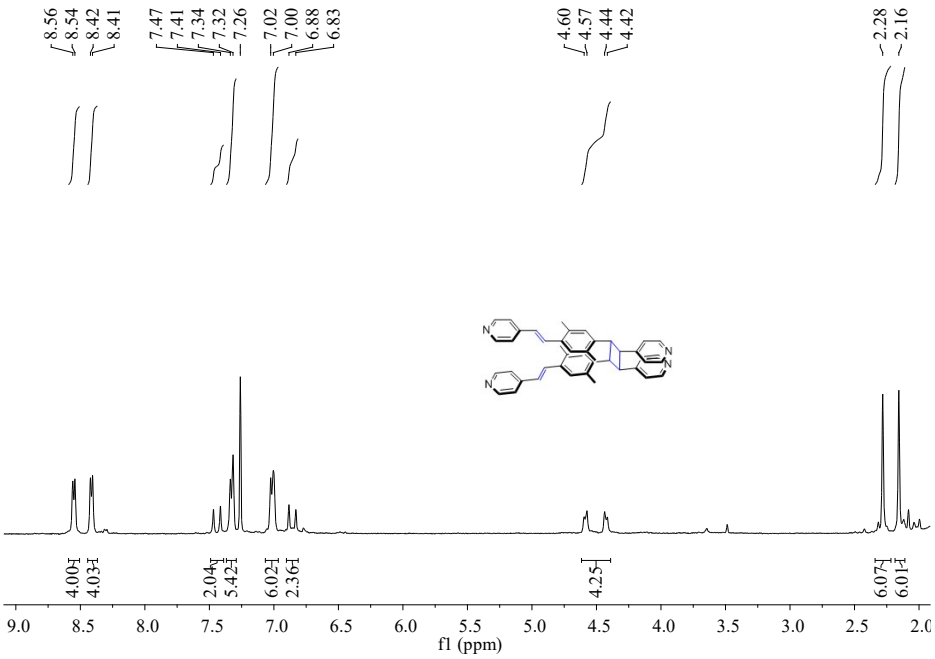

Fig. S6. ^{1}H NMR spectrum of bdpcd ($CDCl_3$).

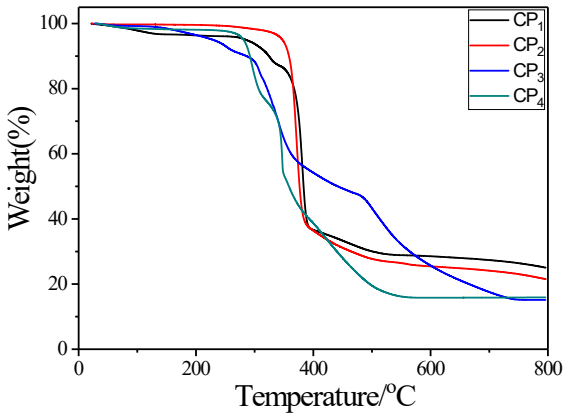

(a)

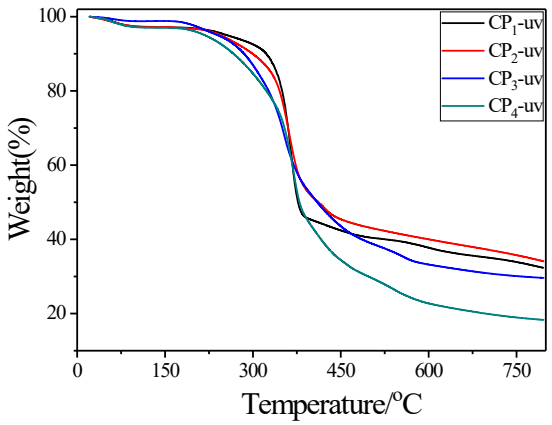

(b)

Fig. S7. Thermogravimetric analysis of **CP_1-CP_4** before (a) and after (b) UV light irradiation.

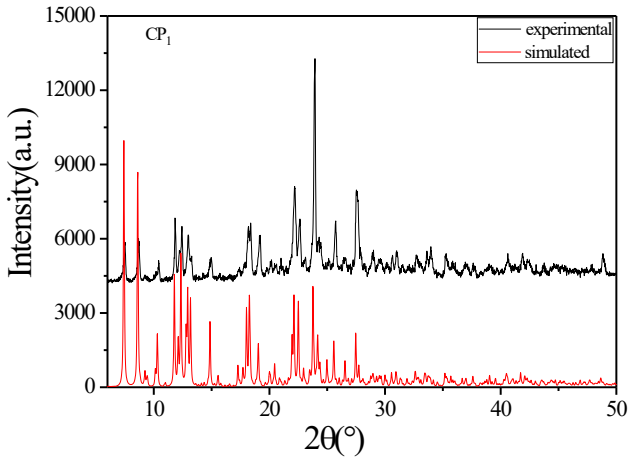
CP1
experimental
simulated
Intensity(a.u.)
2θ(°)
0
3000
6000
9000
12000
15000
10
20
30
40
50

(a)

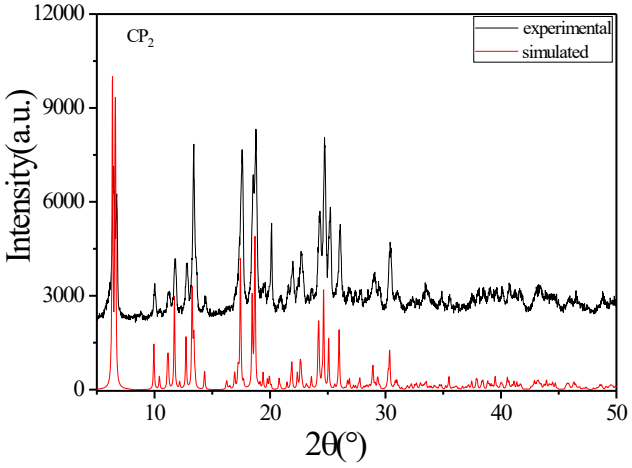
CP2
experimental
simulated
Intensity(a.u.)
2θ(°)
0
3000
6000
9000
12000
10
20
30
40
50

(b)

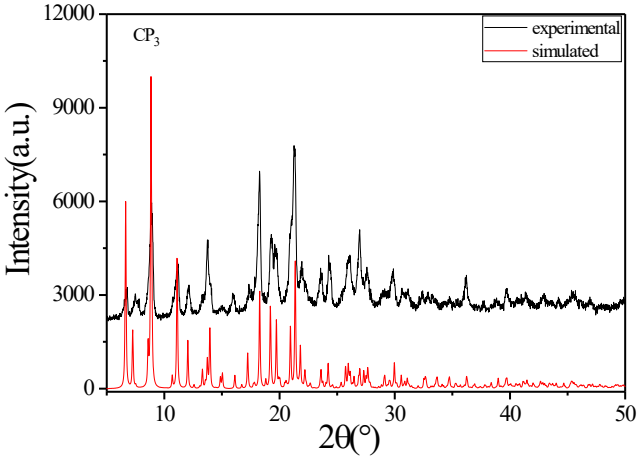
CP3
experimental
simulated
Intensity(a.u.)
2θ(°)
0
3000
6000
9000
12000
10
20
30
40
50

(c)

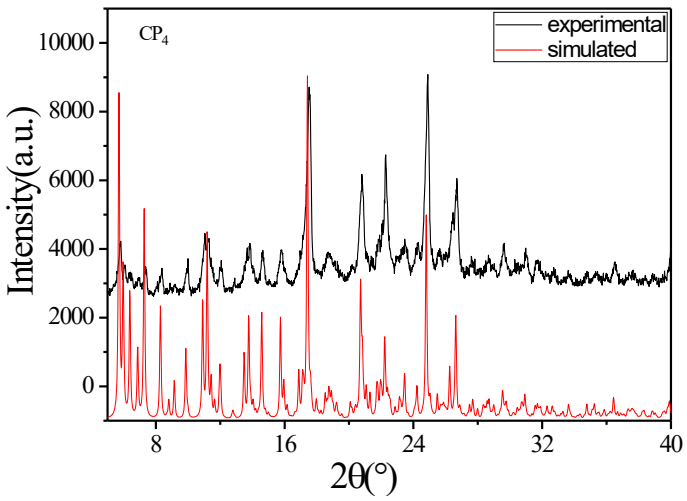

(d)

Fig. S8. The PXRD patterns of **CP$_1$** (a), **CP$_2$** (b), **CP$_3$** (c), **CP$_4$** (d).

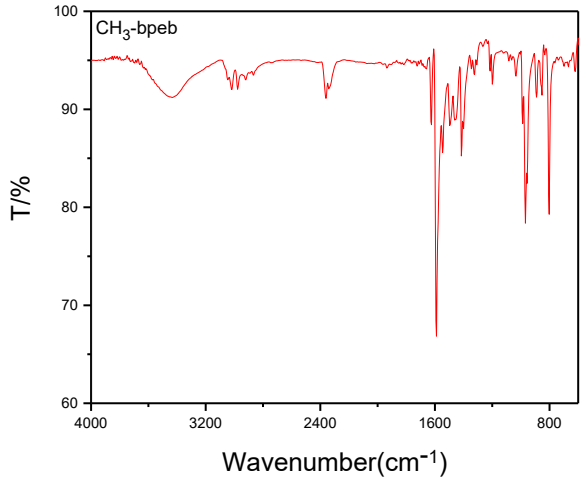

(a)

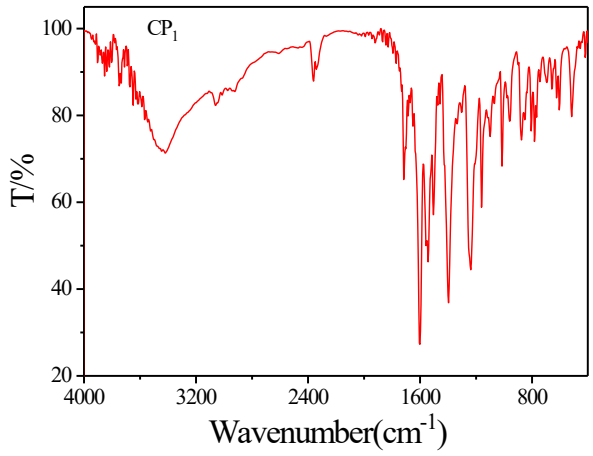

(b)

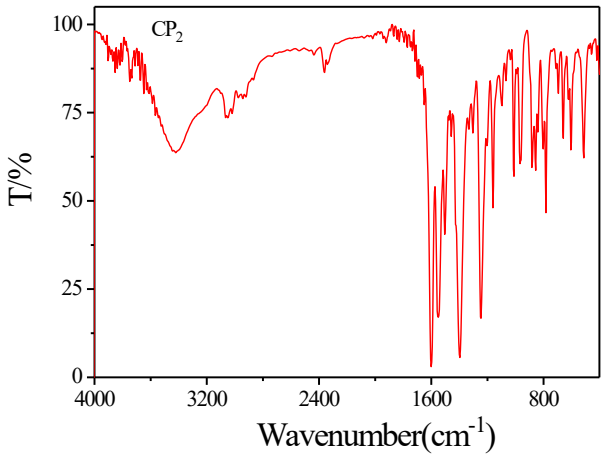

(c)

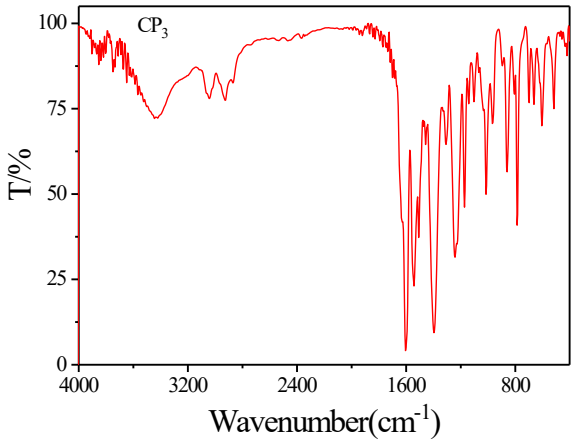

(d)

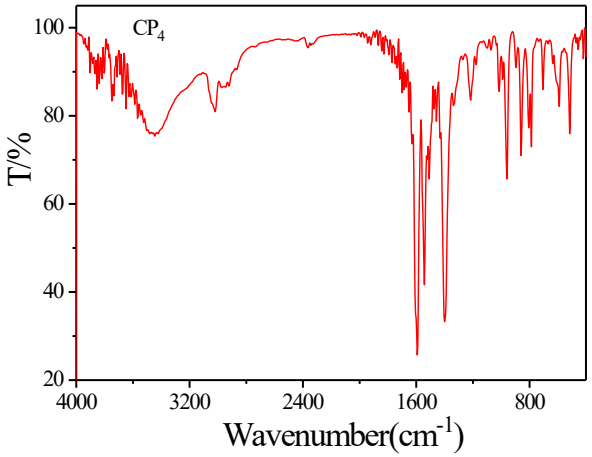

(e)

Fig. S9. IR spectra of CH_3-bpeb (a), **CP_1** (b), **CP_2** (c), **CP_3** (d), **CP_4** (e).

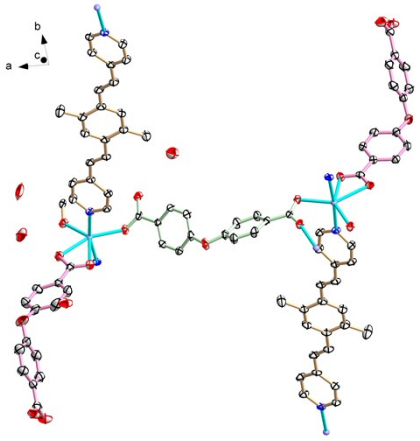

Fig. S10. The asymmetric unit of **CP$_1$**, showing ellipsoids at the 30% probability level.

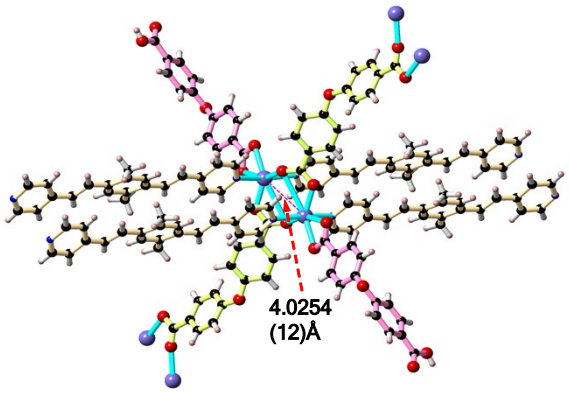

Fig. S11. The coordination environment of Cd (II) in **CP$_1$**.

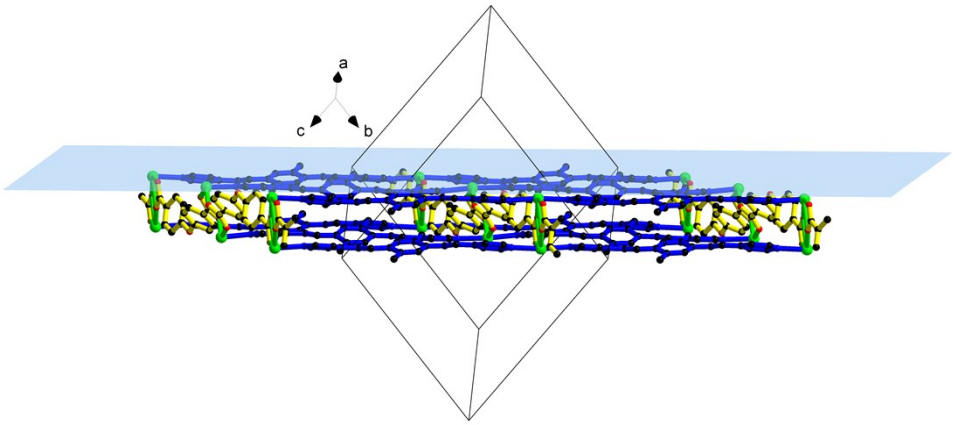

Fig. S12. [$Cd_8(CH_3$-bpeb$)_4$(oba$)_2$] units of **CP$_1$** expand into a 2D layer along the (-122) plane.

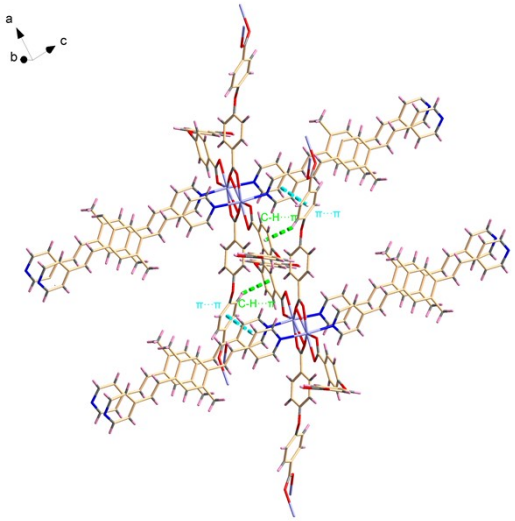

Fig. S13. Adjacent two-dimensional layers in CP_1 are stabilized by π···π and C-H···π interactions.

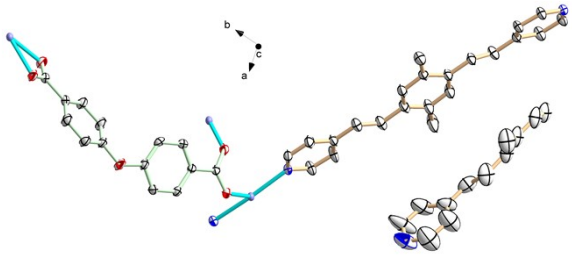

Fig. S14. The asymmetric unit of **CP_2**, showing ellipsoids at the 30% probability level.

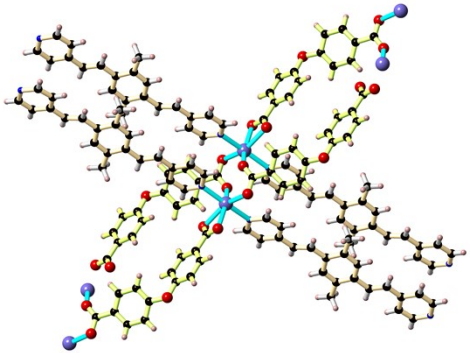

Fig. S15. The coordination environment of Cd (II) in **CP_2**.

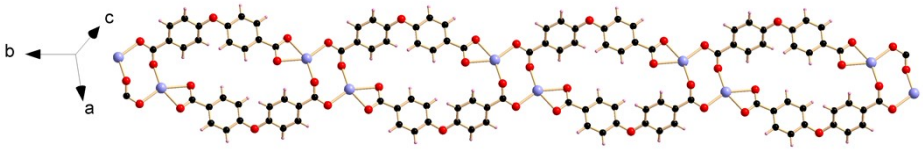

Fig. S16. The ditopic carboxyl ligands of CP_2 extend the structure along the b axis.

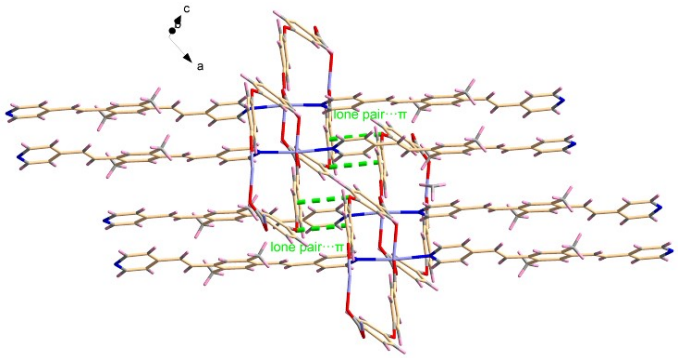

Fig. S17. The adjacent two-dimensional layers in **CP$_2$** are stabilized by lone pair···π interactions.

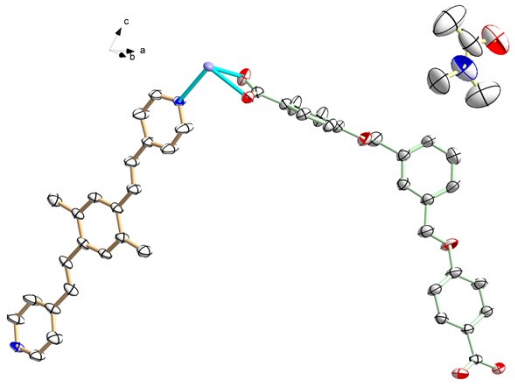

Fig. S18. The asymmetric unit of **CP$_3$**, showing ellipsoids at the 30% probability level.

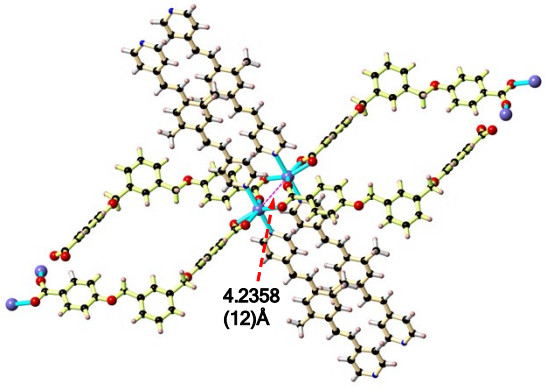

Fig. S19. The coordination environment of Cd (II) in **CP$_3$**.

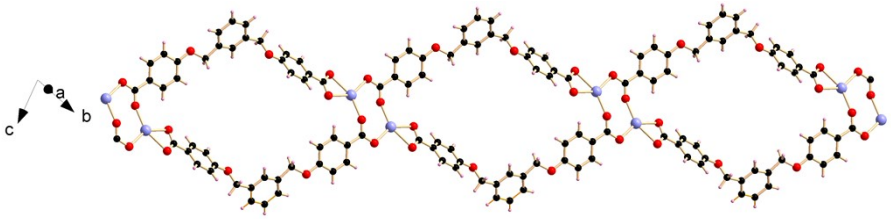

Fig. S20. The rhombic [$Cd_4(pbda)_2$] unit of **CP$_3$** is extended into a 1D chain motif with a corner sharing model.

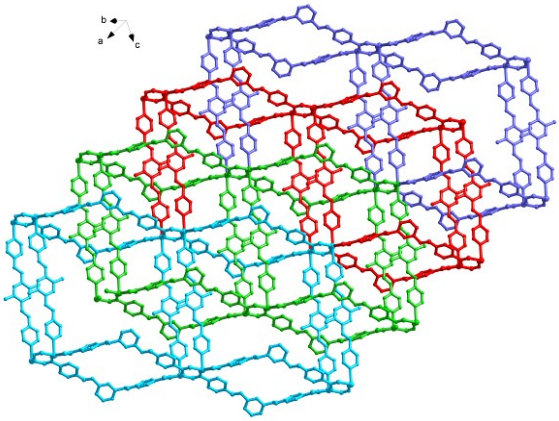

Fig. S21. The 2D layer structure of **CP_3** is packed along the a axis direction.

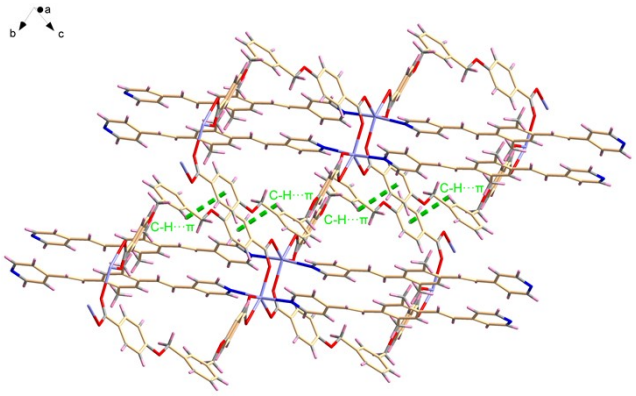

Fig. S22. The adjacent two-dimensional layers in CP_3 are stabilized by C-H···π interactions.

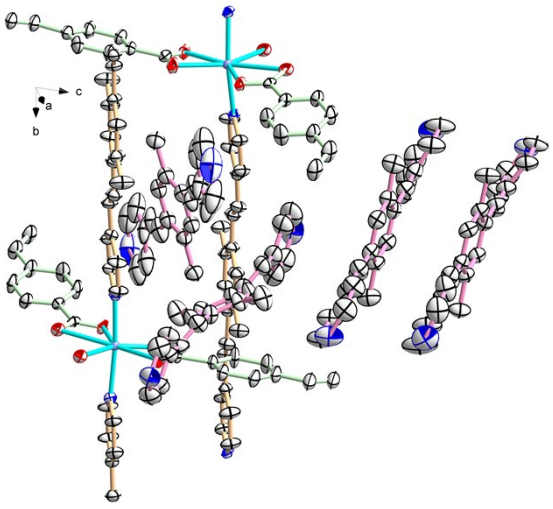

Fig. S23. The asymmetric unit of **CP_4**, showing ellipsoids at the 30% probability level.

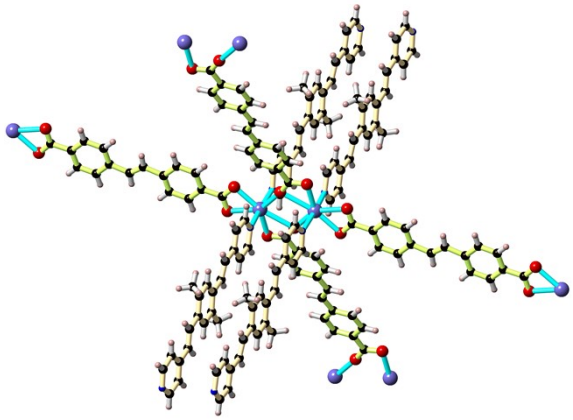

Fig. S24. The coordination environment of Cd (II) in **CP_4**.

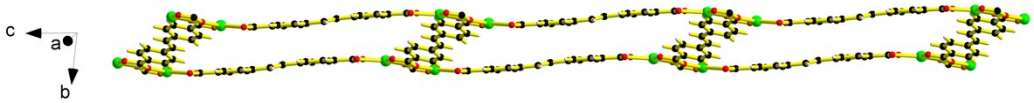

Fig. S25. A wave-like 2D network of $[Cd_8(bpa)_4]$ along c axis.

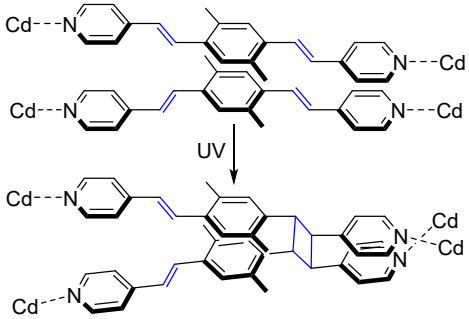

Scheme. S2 Representation of the CH_3-bpeb pairs in structures **CP_1-CP_4**.

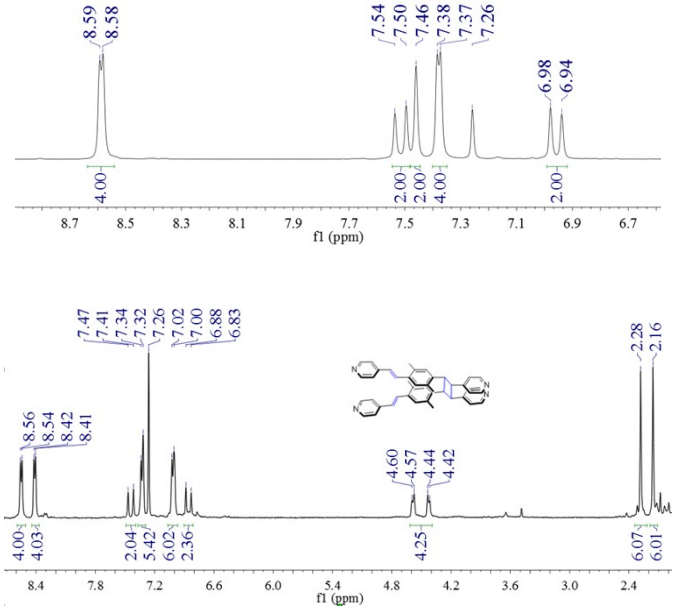

Fig. S26. ^1H NMR spectra of CH_3-bpeb and bdpcd ($CDCl_3$).

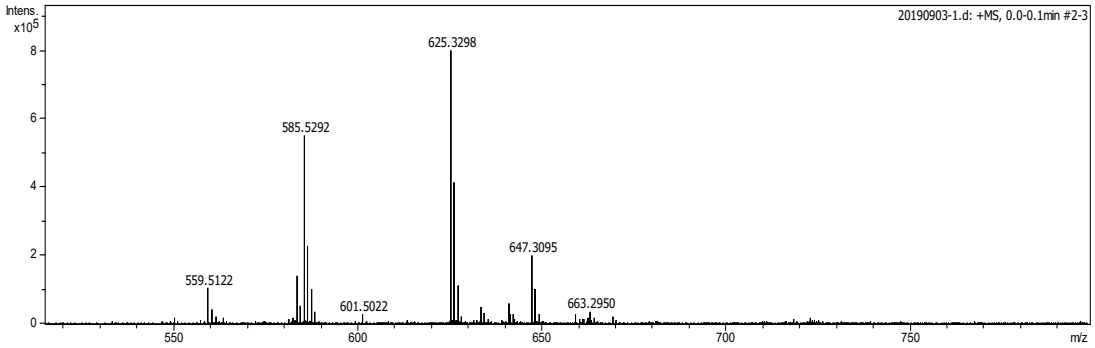

Fig. S27. The mass spectrum of bdpcd.

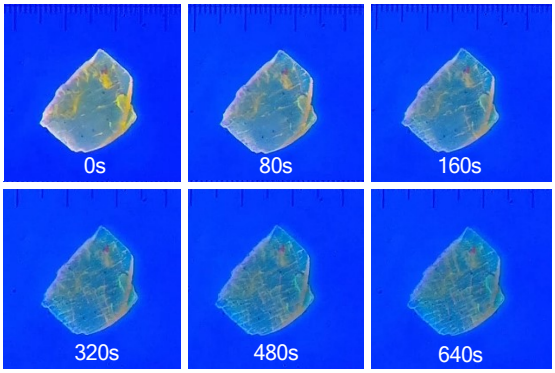

(a)

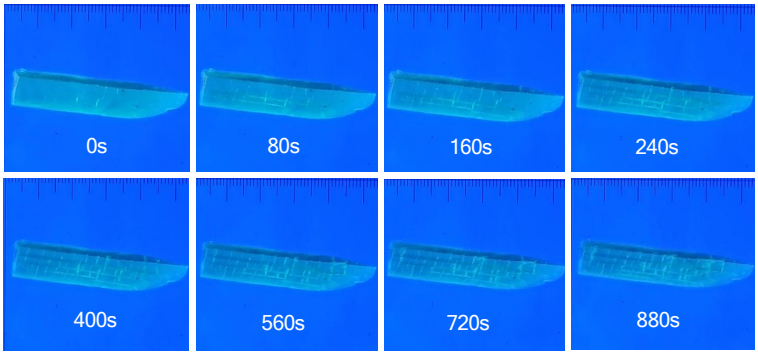

(b)

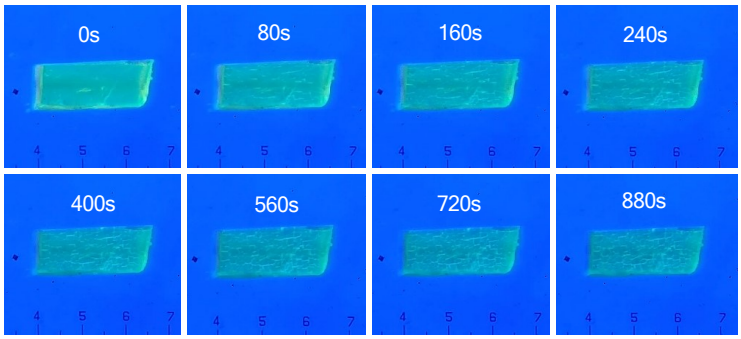

(c)

Fig. S28. Microscopic images of the mechanical response of **CP_1** (a), **CP_3** (b), **CP_4** (c) at different times under 365nm UV lamp irradiation.

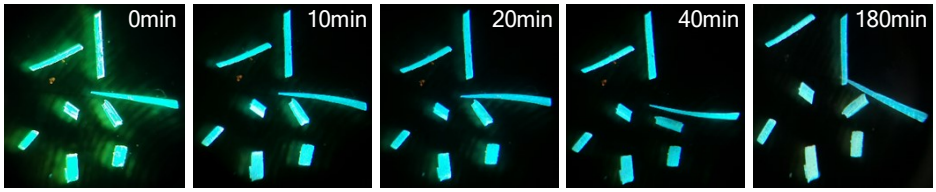

Fig. S29. Microscopic images of the fluorescence contrast of **CP_3** after extended UV illumination times.

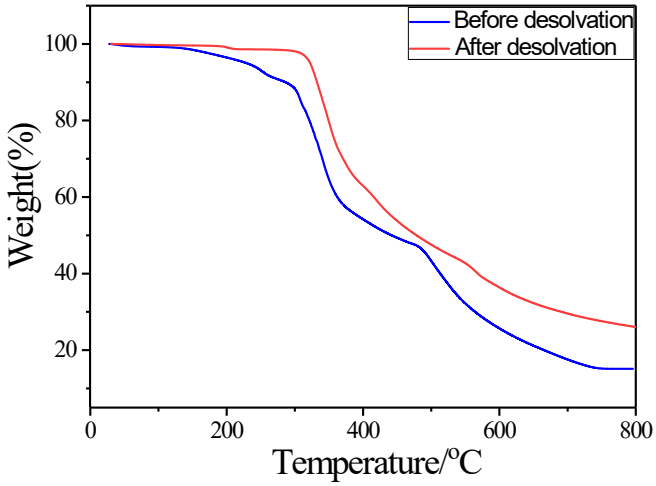

Fig. S30. The thermogravimetric analysis of CP_3 after the crystal was solvent-free.

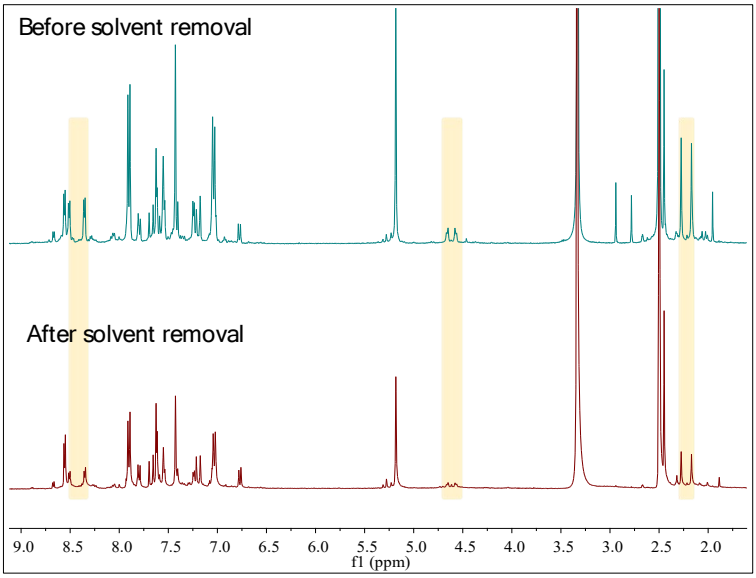

Fig. S31. ^{1}H NMR spectra of **CP_3** before and after desolvation and irradiation under UV light (λ = 365 nm) (d_6-DMSO).

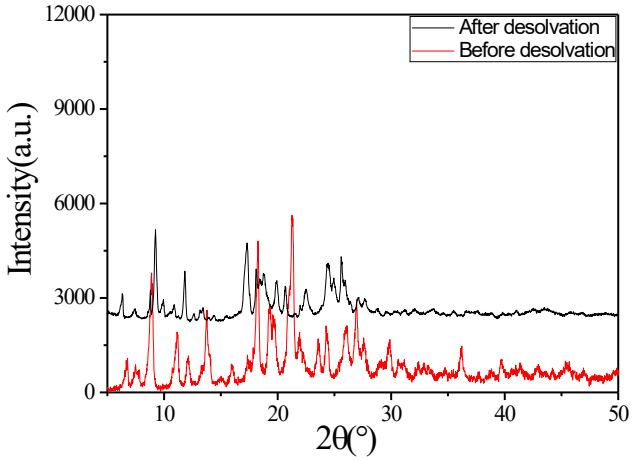

Fig. S32. PXRD patterns of **CP_3** before and after desolvation.

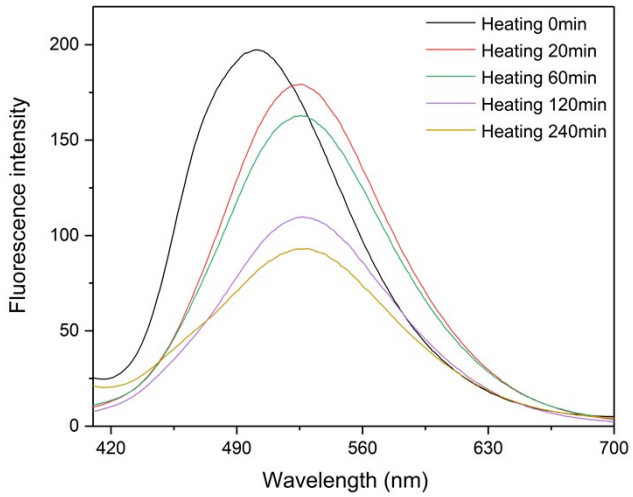

Fig. S33. Solid-state emission spectra of CP_3 after different heating times.

References

1. F. L. Hu, Y. Mi, C. Zhu, B. F. Abrahams, P. Braunstein and J. P. Lang, *Angew. Chem., Int. Ed.*, 2018, **57**, 12696-12701.
2. F. L. Hu, H. F. Wang, D. Guo, H. Zhang, J. P. Lang and J. E. Beves, *Chem. Commun.*, 2016, **52**, 7990-7993.
3. A. C. G. Sheldrick, *Sect. C: Struct. Chem.*, 2015, **71**, 3–8.
4. M. F. Wang, Y. Mi, F. L. Hu, Z. Niu, X. H. Yin, Q. Huang, H. F. Wang and J. P. Lang, *J. Am. Chem. Soc.*, 2020, **142**, 700-704.
5. F. L. Hu, Z. Qin, M. F. Wang, X. W. Kang, Y. L. Qin, Y. Wang, S. L. Chen, D. J. Young and Y. Mi, *Dalton Trans.*, 2020, **49**, 10858-10865.
6. Y. Wang, M. F. Wang, D. J. Young, H. Zhu, F. L. Hu, Y. Mi, Z. Qin, S. L. Chen and J. P. Lang, *Chem. Commun.*, 2021, **57**, 1129-1132.